Title

A Computational and Experimental View of Hydrogen Bonding in Glycerol Water Clusters.

Journal

The journal of physical chemistry. A, 126(10)

ISSN

1089-5639

Authors

Lu, Wenchao
Mackie, Cameron J
Xu, Bo
et al.

Publication Date

2022-03-01

DOI

10.1021/acs.jpca.2c00659

A Computational and Experimental View of Hydrogen Bonding in Glycerol Water Clusters

Wenchao Lu[1], Cameron J. Mackie[1,2], Bo Xu[1], Martin Head-Gordon[1,2 *], and Musahid Ahmed[1 *]

[1] Chemical Sciences Division, Lawrence Berkeley National Laboratory, Berkeley, California 94720, USA

[2] Department of Chemistry, University of California, Berkeley, California 94720, USA

* E-mail: mahmed@lbl.gov; mhg@cchem.berkeley.edu

Abstract

Polyol-water clusters provide a template to probe ionization and solvation processes of paramount interest in atmospheric and interstellar chemistry. We generate glycerol water clusters in a continuous supersonic jet expansion and interrogate the neutral species with synchrotron-based tunable vacuum ultraviolet photoionization mass spectrometry. A series of glycerol fragments (m/z 44, 61, 62, 74) clustered with water are observed. A judicious combination of backing pressure, nozzle temperature, and water vapor pressure allows for tuning the mol % of glycerol. The recorded appearance energies of the water cluster series, m/z 62 and 74 are similar to that observed in pure glycerol, while m/z 61 series show a dependence on cluster composition. Furthermore, this series also tracks the water concentration of the beam. Theoretical calculations on neutral and ionized clusters visualize the hydrogen bond network in these water clusters and provide an assessment of the number of glycerol-glycerol, glycerol-water, and water-water hydrogen bonds in the cluster, as well as their interaction energies. This method of bond counting and interaction energy assessment explains the changes in the mass spectrum as a function of mol % and offers a glimpse of the disruption of the hydrogen bond network in glycerol-water clusters. The calculations also reveal interesting barrier-less chemical processes in photoionized glycerol water clusters that are either activated or do not occur without the presence of water. Examples include spontaneous intramolecular proton transfer within glycerol to form a distonic ion, non-activated breaking of a C-C bond, and spontaneous proton transfer from glycerol to water. These results appear relevant to radiation-induced chemical processing of alcohol-water ices in the interstellar medium.

Introduction:

Glycerol contains three hydroxyl groups and is miscible with water. It is a key molecular building block of lipids and is used as a cryo-protectant to stabilize molecules, cells, and tissues under cooling to subzero temperatures.[1] As a result, it plays important roles in biotechnology, plant and animal breeding, the pharmaceutical industry, and modern medicine. In the chemical industry, glycerol formed from biodiesel is catalytically processed in the aqueous phase to form value-added marketable commodities. Structural evidence of the effect of glycerol on protein hydration and thermal structure transition has been reported.[2] Polyols such as glycerol have been implicated in aerosol formation[3] and chemistry in the atmosphere and in electronic cigarettes[4] while it has been suggested that its interactions with water can play a crucial role by driving phase transitions and diffusional dynamics. Their relevance to astrochemistry[5, 6] arises from the detection of sugar alcohols in interstellar matter and have been implicated as foundational molecules which could lead to the origins of life.

To understand how glycerol functions as a cryo-protectant, the physical properties of glycerol and its mixtures with water have been studied extensively both experimentally and theoretically. Neutron scattering and molecular dynamics simulations suggest that glycerol and water form clusters which is directed by intramolecular and intermolecular hydrogen bonding between the two systems.[7, 8] Infrared,[9-11] and dielectric[12-14] spectroscopy of water-glycerol mixtures also infer a concept of clusters, confinement and extensive changes in the hydrogen bond network between these two liquids as a function of concentration. Recently, a molecular level picture of the hydrogen bond network was revealed using X-Ray photoelectron spectroscopy of aqueous glycerol aerosols in conjunction with IR and THz spectroscopy of mixed solutions.[15] Therein, it was shown that upon increasing the glycerol content, the hydrogen bond network evolved from glycerol molecules being surrounded by water forming a solvated water network, towards one where water is confined within glycerol's hydrogen bond network. Beyond a mole fraction of 22% glycerol, the aerosols resembled bulk glycerol. The picture that emerges from these studies in aerosols and solutions is one of embedded clusters in a hydrogen bond network.

To quantify this hydrogen bonding at the molecular level, we performed a photoionization mass spectrometry study of glycerol water clusters in a molecular beam coupled with theoretical calculations on both neutral and ionized glycerol water clusters. There have been early theoretical calculations[16] of gas-phase glycerol and its interactions with water. Also, we note that there have been field ionization[17] and electron impact ionization[18] studies of glycerol and its clusters. Glycerol ionization has been invoked

in a case of surface ionization of liquid glycerol by sodium ions,[19, 20] and also VUV photoionization of glycerol have been undertaken in aerosols.[21, 22] We have studied the photoionization of glycerol molecules and its dimer in the gas phase using synchrotron-based vacuum ultraviolet (VUV) photoionization mass spectrometry.[23] Our combined experimental and theoretical study of glycerol water cluster photoionization presented here builds upon this framework and also complements the X-Ray, IR, and THz study performed on aqueous glycerol aerosols.[15]

Methods

Experimental Details

The experiments are performed with a reflectron time-of-flight mass spectrometer incorporating a continuous supersonic expansion molecular beam source. The apparatus is coupled to a 3-meter vacuum monochromator on the Chemical Dynamics Beamline (9.0.2) located at the Advanced Light Source and has been described in our previous studies.[24-26] Briefly, glycerol was placed at the front end of a stainless-steel nozzle, which has a 50 µm diameter center hole, and is heated to 408 K using a cartridge heater. Glycerol vapor is diffused into 800 Torr argon carrier gas seeded with water vapor. The gas mixture passes through the 50 µm hole and expands supersonically in vacuum to produce a molecular beam at the interaction region of a reflectron time-of-flight mass spectrometer where the neutral clusters are ionized by the VUV light and subsequently detected. Mass spectra are recorded for the photon energy range between 8 and 12.5 eV in photon energy step size of 50 meV. The photoionization efficiency (PIE) curves of the glycerol-water clusters are obtained by integrating over the peaks in the mass spectrum at each photon energy, and are normalized by the photon flux.

Computational Details

Theoretical calculations are carried out for various $(Gly)_x + (H_2O)_y$ cluster sizes, with *x* ranging from one to three, and *y* ranging from zero to five. $(Gly)_3 + (H_2O)_5$ is skipped in favor of a more relevant glycerol-water mass ratio provided by $(Gly)_3 + (H_2O)_8$. The neutral glycerol-water cluster conformers are obtained through a conformer distribution search using the Spartan chemical software package.[27] The software uses a Merck Molecular Force Field (MMFF)[28] model in conjunction with a Monte Carlo search procedure. For each cluster size, three separate Monte Carlo searches are performed, each starting from a random non-equilibrium geometry. After 3000 steps, the searches are terminated and the lowest 100 conformers are retained. The results from the separate searches are then combined and the duplicates removed. The

lowest 30 conformers for each cluster size are then re-optimized using the ωB97X-D/6-311+G(2d,p) functional/basis set combination. The ωB97X-D functional was chosen for its range-separated exact exchange and dispersion corrections, which yield quite good performance for intermolecular interactions.[29] The geometries of the ionized clusters are obtained by re-optimizing the structures of the lowest-energy neutral conformers at the ωB97X-D/6-311+G(2d,p) with the total charge set to +1. Single-point calculations at the ωB97X-V/def2-TZVPPD level of theory (a more modern functional with a larger atomic orbital basis set) were then carried out. The interaction energies of the shortest hydrogen bonds within each cluster were calculated using third-order effective 2-body interaction energies as described recently.[30]

Results and Discussion:

Experimental:

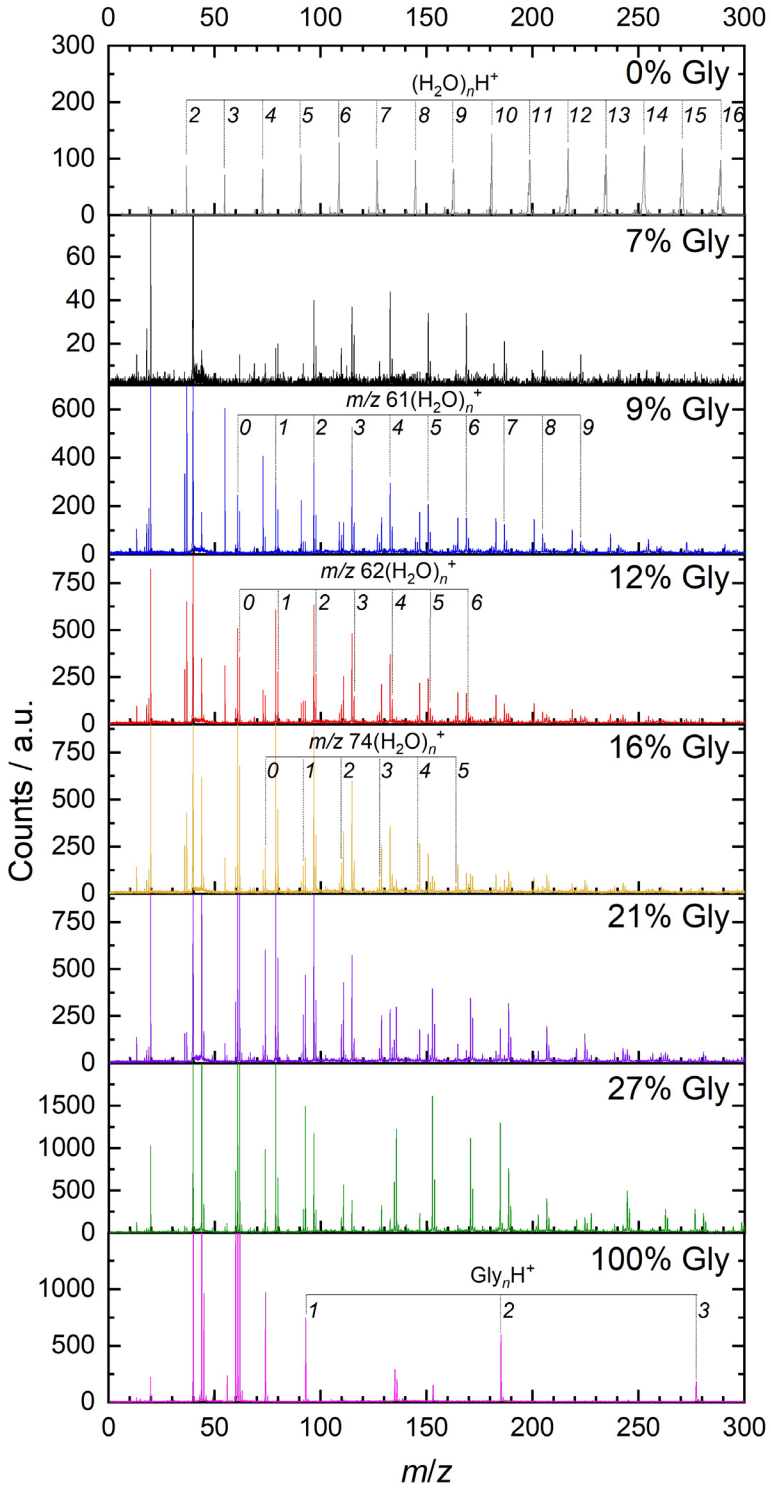

Figure 1: Intensities of glycerol water clusters recorded at 10.5 eV at various concentrations. The mass spectrum of pure water clusters is collected at 12.0 eV.

By tuning the source conditions, notably, the temperature of the nozzle and water reservoir, coupled with the pressure of backup Ar gas, the glycerol to water concentration in the beam can be changed. Figure 1

shows the mass spectra recorded at 10.5 eV for six different mole fractions of glycerol (Gly%) in glycerol-water mixtures, namely, 7%, 9%, 12%, 16%, 21% and 27%, together with that of pure water clusters collected at 12.0 eV due to the high-lying ionization energies of water clusters. For unmixed water or glycerol, clusters beyond $(H_2O)_{16}$ or $(Gly)_3$ are formed but are not shown in the figure. Note that the H_2O monomer has an ionization energy of 12.6 eV and will not be seen in a 12.0 eV spectrum. For mixed systems, at the highest glycerol concentration of 27%, the fragmentation patterns are mostly that of pure glycerol and the intensity of water seeded glycerol clusters decrease rapidly as the mass increases, while with increasing water content, glycerol-water clusters [m/z $61(H_2O)_{0-10}]^+$, [m/z $62(H_2O)_{0-10}]^+$, and [m/z $74(H_2O)_{0-9}]^+$ dominate the spectrum. The distributions of [m/z $62(H_2O)_{0-10}]^+$, and [m/z $74(H_2O)_{0-9}]^+$ decrease as the cluster size increases, while [m/z $61(H_2O)_{0-10}]^+$ clusters shows the maximum at [m/z $61(H_2O)_{2-4}]^+$. These cluster series indicate the preferred fragmentation pattern upon photoionization. It is worth mentioning that [m/z $74(H_2O)_{0-9}]^+$ series may contain the contribution of hydrated glycerol, $[Gly(H_2O)_{0-8}]^+$ because of the same mass these two series share.

Our experimental discussion of the mass spectra of glycerol water clusters upon photoionization will be guided by previous results of fragmentation of the glycerol monomer and dimer in the absence of water.[23] The primary fragments in glycerol monomer are m/z 44, 45, 60, 61, 62 and 74. In the case of the dimer, additional peaks are observed in m/z 93, 135, 136, 153 and 185. In both cases, the presence of the non-fragmented monomer (m/z 92) and dimer (m/z 184) is miniscule, and can be explained by extensive dissociative photoionization mediated via strong hydrogen-bonded ion complexes. Clustering between glycerol leads to the absence of water elimination and an enhancement in proton transfer upon ionization, which favors the formation of Gly_nH^+ type ions. This should be contrasted with what is observed when dissociative ionization occurs from glycerol water clusters. The series observed for m/z 44 or 62, 61 and 74 are all non-protonated species originating from water clusters being bound to the original fragments. One can also surmise the energetics of these processes by comparing the appearance energies of particular fragments. For m/z 74, which occurs from water elimination from the glycerol parent, we observe an appearance energy (AE) of 9.8 eV, which is very similar to that observed for the monomer. For m/z 62, corresponding to formaldehyde loss, the AE of 9.7 eV corresponds well with the monomer again. Finally, for m/z 44, the AE is similar to that observed in the monomer, corresponding to vinyl alcohol elimination is also similar at 10.3 eV.

The appearance of series [m/z $61(H_2O)_{0-4}]^+$, [m/z $62(H_2O)_{0-4}]^+$, [m/z $74(H_2O)_{0-3}]^+$, and [m/z 93 $(H_2O)_{0-2}]^+$ are also tracked as a function of photon energy shown in Table 1, with their photoionization efficiency (PIE)

curves presented in the **Supplementary Information**. The AE of each species across different Gly% are very consistent, indicating the concentration of water did not change the fragmentation pattern of these composite clusters. Our current measurements are also very consistent to our previous results of glycerol photoionization.[23] The appearance energies within a series gradually decrease and then converge to a specific value as the number of water molecules attached increases, similar to pure water clusters.[26] A very similar observation for such series has been observed in PAH water clusters[31] and in nucleobase water clusters.[32] There a case was made that these series originate from the ionization of the 3A" water orbital. This observation provides a hint as to the ionization process and the hydrogen bond network of the glycerol water clusters. The series $[m/z\ 74(H_2O)_{0\text{-}3}]^+$ have very similar PIE curves with an origin around 9.7 eV. Series $[m/z\ 62(H_2O)_{0\text{-}4}]^+$ has an onset around 9.6 – 9.8 eV, and could either originate from m/z 44 (onset of 10.25 eV) or m/z 62 (onset of 9.8 eV). The series $[m/z\ 61(H_2O)_{0\text{-}4}]^+$ has onsets that are significantly dependent on the number of water molecules present, as 10.4 for dry $[m/z\ 61(H_2O)_0]^+$ to 9.5 for $[m/z\ 61(H_2O)_4]^+$.

Table 1: The experimental appearance energies as a function of mole fraction of Glycerol in the mixture, in comparison to those of glycerol (from ref [23])

	Appearance Energy (eV) as a Function of Gly%				Appearance Energy (eV) of Glycerol from **Ref. [23]**	
	7%	16%	27%	100%	Experimental	Calculated
m/z 44	10.1	10.2	10.3	10.2	10.3	10.44
m/z 62	9.8	9.8	9.9	9.9	9.9	9.72
m/z $62(H_2O)^+$	9.8	9.6	9.6			
m/z $62(H_2O)_2^+$	9.7	9.6	9.6			
m/z $62(H_2O)_3^+$	9.7	9.6				
m/z $62(H_2O)_4^+$	9.7	9.6				
m/z 61	10.3	10.4	10.4	10.4	10.3	10.34
m/z $61(H_2O)^+$	10.0	9.9	9.9			
m/z $61(H_2O)_2^+$	9.7	9.6	9.6			
m/z $61(H_2O)_3^+$	9.7	9.6	9.6			
m/z $61(H_2O)_4^+$	9.6	9.5				
m/z 74	9.7	9.7	9.8	9.8	9.8	9.72
m/z $74(H_2O)^+$	9.7	9.6	9.6			
m/z $74(H_2O)_2^+$	9.6	9.7	9.5			
m/z $74(H_2O)_3^+$		9.6				
m/z 93		10.5	10.5	10.6	10.5	
m/z $93(H_2O)^+$		10.4	10.3			
m/z $93(H_2O)_2^+$		10.4	10.3			

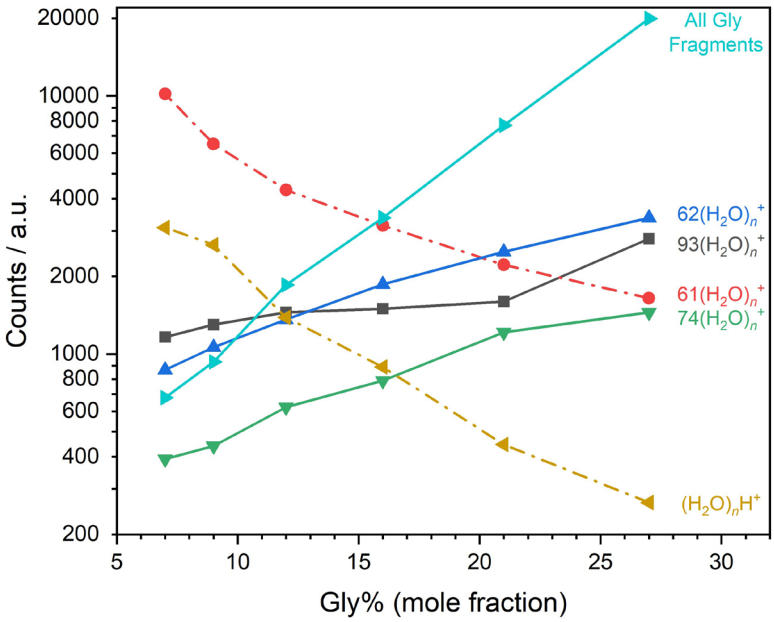

Figure 2: Sum of intensities of each cluster series as a function of Gly%, recorded at 12.0 eV.

Figure 2 shows the trend of the sum of various fragment series of glycerol water clusters photoionized at 12.0 eV and provides a snapshot of what the population of clusters is upon expansion and how the hydrogen bond network evolves across the concentration series. The summed series dependence also provides a clue towards the origin of the [m/z $61(H_2O)_n]^+$series. With the increase of glycerol concentration, we see the series of [m/z $62(H_2O)_n]^+$, [m/z $74(H_2O)_n]^+$ and [m/z $93(H_2O)_n]^+$ track glycerol, while [m/z $61(H_2O)_n]^+$ appears to follow the depletion of water in the beam, which suggests this series is directly implicated in glycerol water photoionization dynamics. Recall that earlier we mentioned that [m/z $61(H_2O)_n]^+$ series appearance energies also changed with the number of water molecules attached to them. Our computational calculations detailed later also provide evidence of how water affects the fragmentation dynamics of photoionized glycerol water clusters.

Computational:

The geometries are presented in Figure 3 from which the number of glycerol-glycerol, glycerol-water, and water-water bonds for the lowest energy conformers were extracted as summarized in Table 2. The shortest hydrogen bond lengths of each conformer are presented in Table 3. The third-order effective two-body interaction energies between the molecules containing the shortest hydrogen bonds are

presented in Table 4; when multiple hydrogen bonds are present between the two bodies, the values in Table 4 are normalized by the number of hydrogen bonds.

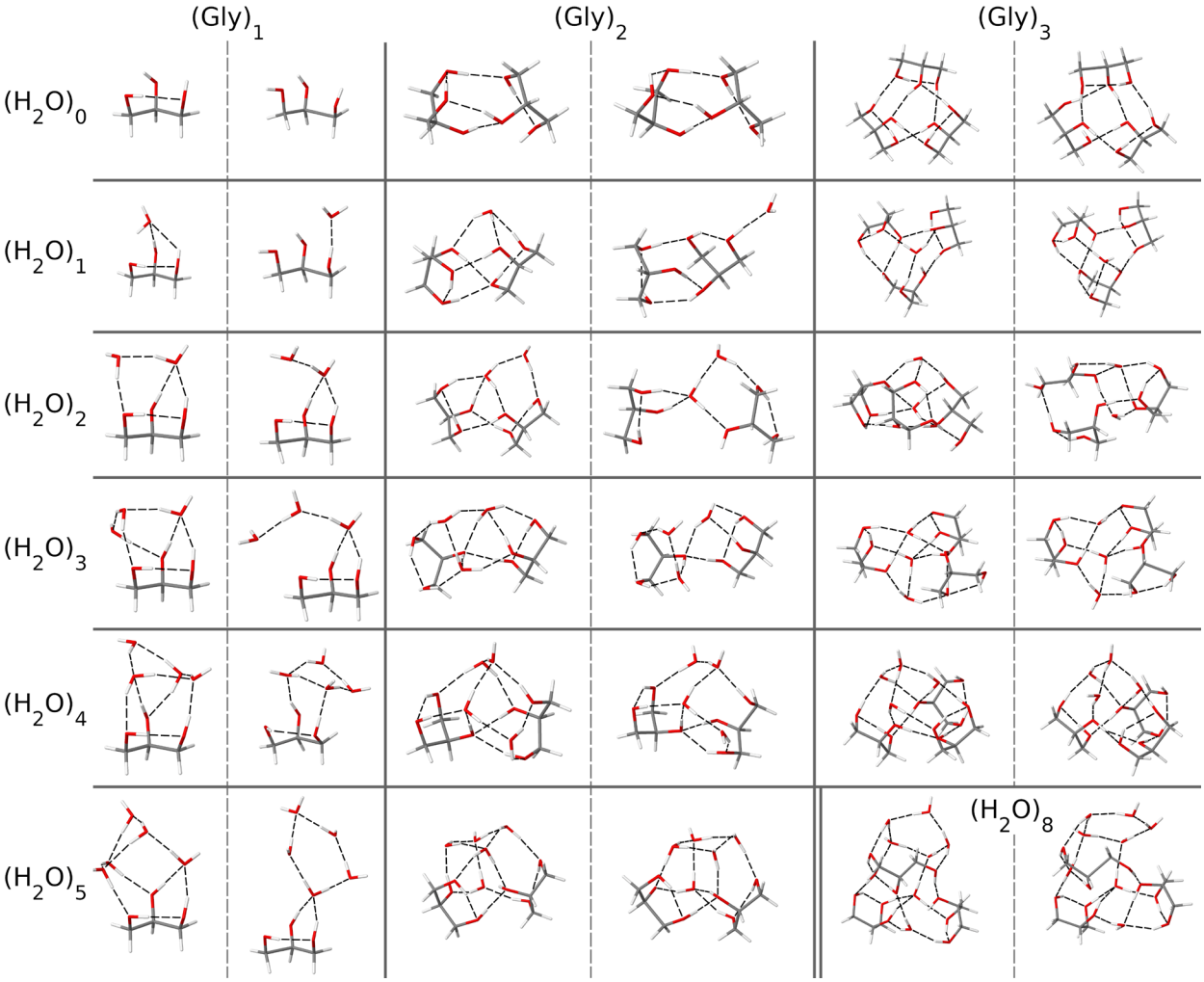

Figure 3: The lowest energy conformers of neutral $(Gly)_x^+$ $(H_2O)_y$ with the corresponding structures of the relaxed cations. Within each row and column, the optimal neutral cluster is shown to the left of the optimal cationic cluster.

Table 2: The number of glycerol-glycerol (GG), glycerol-H_2O (GW), and H_2O-H_2O (WW) hydrogen bonds in the computed minimum energy conformers found in this work. Listed are the values for the neutral structures and the corresponding ionized structures, as well as the change in number of hydrogen bonds from neutral to cation (Δ).

		Neutral			Cation			Δ		
$(Gly)_x$	$(H_2O)_y$	GG	GW	WW	GG	GW	WW	GG	GW	WW
1	0	-	0	-	-	-	-	-	-	-
1	1	-	2	-	-	1	-	-	-1	-
1	2	-	3	1	-	2	1	-	-1	0
1	3	-	4	2	-	2	2	-	-2	0
1	4	-	3	4	-	2	4	-	-1	0
1	5	-	4	5	-	2	5	-	-2	0
2	0	3	-	-	3	-	-	0	-	-
2	1	3	3	-	3	1	-	0	-2	-
2	2	2	4	1	0	4	1	-2	0	0
2	3	1	6	2	1	5	1	0	-1	-1
2	4	2	7	3	2	5	3	0	-2	0
2	5	1	7	5	1	6	5	0	-1	0
3	0	6	-	-	6	-	-	0	-	-
3	1	4	4	-	4	3	-	0	-1	-
3	2	3	7	0	2	6	0	-1	-1	0
3	3	2	9	1	1	8	1	-1	-1	0
3	4	3	7	3	3	5	3	0	-2	0
3	8	1	11	7	1	9	7	0	-2	0

Table 3: The lengths of the shortest glycerol-glycerol (GG), glycerol-H_2O (GW), and H_2O-H_2O (WW) hydrogen bonds in the lowest energy conformers of glycerol-water clusters and their corresponding cations.

		Neutral [Å]			Cation [Å]		
$(Gly)_x$	$(H_2O)_y$	GG	GW	WW	GG	GW	WW
1	0	-	-	-	-	-	-
1	1	-	1.885	-	-	1.629	-
1	2	-	1.787	1.748	-	1.633	1.717
1	3	-	1.836	1.688	-	1.597	1.623
1	4	-	1.837	1.691	-	1.609	1.640
1	5	-	1.716	1.641	-	1.520	1.629
2	0	1.818	-	-	1.524	-	-
2	1	1.837	1.824	-	1.487	1.758	-
2	2	1.786	1.776	1.842	-	1.525	1.628
2	3	1.832	1.747	1.787	1.533	1.578	1.659
2	4	1.821	1.732	1.652	1.576	1.582	1.601
2	5	1.882	1.736	1.684	1.682	1.738	-
3	0	1.780	-	-	1.471	-	-
3	1	1.867	1.826	-	1.521	1.692	-
3	2	1.694	1.752	-	1.512	1.752	-
3	3	1.850	1.763	1.819	1.442	1.691	1.991
3	4	1.742	1.796	1.685	1.477	1.479	1.718
3	8	1.554	1.771	1.594	1.495	1.594	1.677

Table 4: The hydrogen bond interaction energies which contain the shortest hydrogen bonds between glycerol-glycerol (GG), glycerol-H_2O (GW), and H_2O-H_2O (WW) of the lowest energy conformers of the glycerol-water clusters and their corresponding cations, normalized by the number of interacting hydrogen bonds.

		Neutral [kcal/mol]			Cation [kcal/mol]		
$(Gly)_x$	$(H_2O)_y$	GG	GW	WW	GG	GW	WW
1	0	-	-	-	-	-	-
1	1	-	-6.90	-	-	-21.2	-
1	2	-	-10.5	-6.71	-	-12.5	-5.51
1	3	-	-5.47	-7.01	-	-13.3	-6.15
1	4	-	-8.88	-	-	-19.5	-5.34
1	5	-	-8.22	-6.62	-	-15.1	-5.22
2	0	-7.13	-	-	-16.5	-	-
2	1	-7.37	-6.12	-	-17.3	-8.00	-
2	2	-10.2	-7.20	-4.32	-	-14.9	-4.23
2	3	-9.75	-6.75	-5.77	-23.9	-6.86	-6.72
2	4	-5.95	-6.65	-7.14	-13.2	-9.55	-6.02
2	5	-8.02	-8.45	-7.14	-	-6.20	-
3	0	-15.8	-	-	-26.9	-	-
3	1	-7.77	-8.52	-	-13.2	-4.23	-
3	2	-	-3.07	-	-32.4	-	-
3	3	-6.05	-6.35	-5.00	-24.1	-4.11	-2.88
3	4	-12.2	-4.93	-6.93	-30.8	-11.4	-6.31
3	8	-8.63	-4.35	-7.36	-22.4	-12.9	-6.19

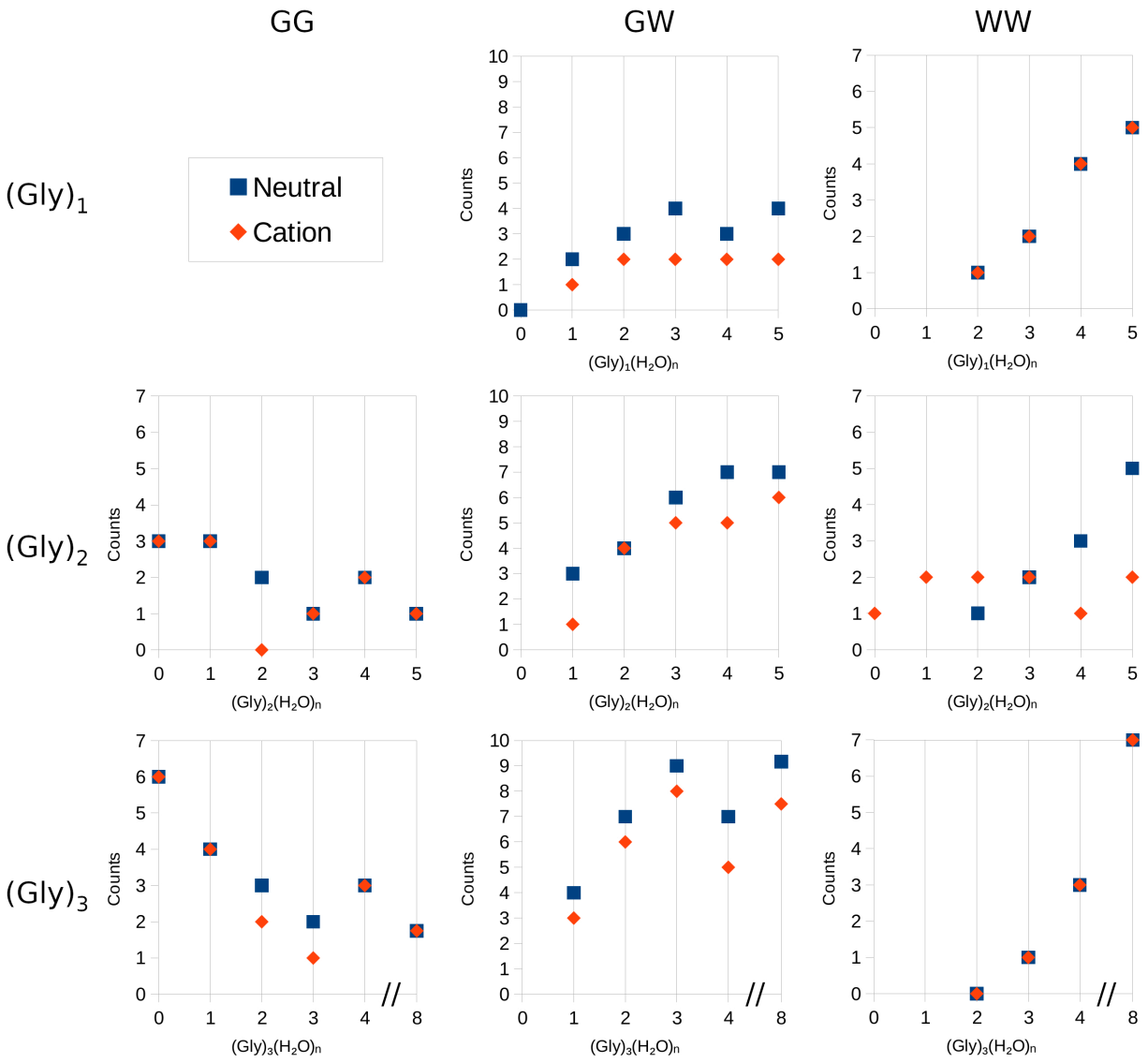

Figure 4: The number of glycerol-glycerol (GG), glycerol-H_2O (GW), and H_2O-H_2O (WW) hydrogen bonds in the computed minimum energy conformers found in this work. Listed are the values for the neutral structures and the corresponding ionized structures, drawn from Table 3.

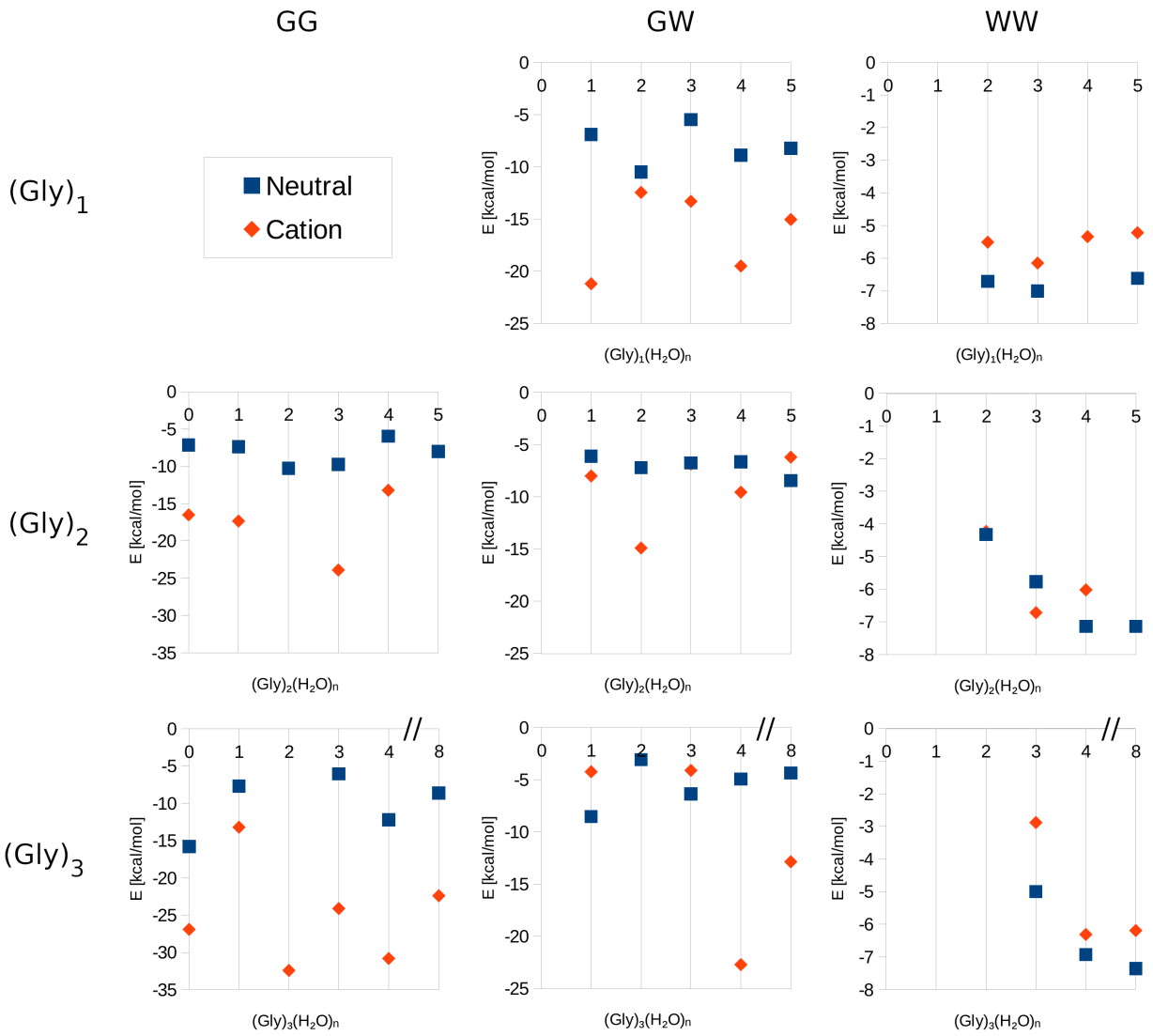

Figure 5: The interaction energies of glycerol-H_2O, glycerol-glycerol, and H_2O-H_2O hydrogen bonds in the computed minimum energy conformers found in this work. Listed are the values for the neutral structures and the corresponding ionized structures, drawn from Table 4.

It is worth noting that for the neutral systems, as the number of hydrogen-bonded water increases, the numbers of glycerol-water (GW) and water-water (WW) bonds follow the same trend while the number of glycerol-glycerol (GG) bonds decreases. The cation cases have the similar numbers of those three types of hydrogen bonds, with the numbers being only 1-2 fewer than those of the neutral case (Table 2 and Figure 4).

Table 4 and the corresponding Figure 5 show distinct behavior of the GG, GW and WW bonds upon ionization and across glycerol concentrations. The GG bonds are strengthened upon ionization, with an

increase in bonding energy with the increase of glycerol concentration. At $(Gly)_2$ an average increase of 10.3 kcal/mol is observed, with a maximum increase of 14.1 kcal/mol; while at $(Gly)_3$ an average increase of 13.4 kcal/mol is observed with a maximum increase of 18.6 kcal/mol. The opposite trend is observed for the GW bonds, the increase in the bonding strength upon ionization is lower with increasing glycerol concentrations. At $(Gly)_1$ an average increase of 8.3 kcal/mol is observed, with a maximum increase of 14.3 kcal/mol; at $(Gly)_2$ an average increase of only 2.1 kcal/mol is observed, with a maximum increase of 7.7 kcal/mol, however a *decrease* of 2.3 kcal/mol is seen at $(Gly)_2(H_2O)_5$; at $(Gly)_3$ an average increase of 2.1 kcal/mol is observed, with a maximum increase of 8.5 kcal/mol seen with $(Gly)_3(H_2O)_8$, however *two decreases* in bonding energy are seen at $(Gly)_3(H_2O)_1$ and $(Gly)_3(H_2O)_3$ of 4.3 kcal/mol and 2.2 kcal/mol respectively. For the WW hydrogen bonds, no clear trends across the glycerol concentrations are present, however in each case (excluding $(Gly)_2(H_2O)_3$), ionization leads to an average weakening of bonding energies of 1.1 kcal/mol, with a maximum decrease of 2.1 kcal/mol at $(Gly)_3(H_2O)_3$.

For most cases, no trends across H_2O concentrations are observed, except for the WW hydrogen bonds themselves. For the neutral clusters, a cooperative effect is observed whereby individual WW hydrogen bonds increase in strength with the addition of H_2O neighbors, as seen in previous work.[30] This cooperative effect leads to an increase in bonding energy from 4.8 kcal/mol for an isolated H_2O dimer, to 7.1 kcal/mol beyond approximately $(H_2O)_3$, in agreement with the previous study.

The ionization process, therefore mostly influences the GW bonds. These facts indicate that the GW hydrogen network is weakened and broken, while the GG network is strengthened, and the WW network is largely unaffected. This might correlate to Figure 2 in that the $[m/z\ 62(H_2O)_n]^+$, $[m/z\ 74(H_2O)_n]^+$ and $[m/z\ 93(H_2O)_n]^+$ series increase along with higher Gly%, whereas $[m/z\ 61(H_2O)_n]^+$ series decrease along with higher Gly%. From Table 2, the number of GG bonds follow the same trend of m/z $[m/z\ 62(H_2O)_n]^+$, $[m/z\ 74(H_2O)_n]^+$ and $[m/z\ 93(H_2O)_n]^+$ series, whereas the numbers of GW and WW bonds follow $[m/z\ 61(H_2O)_n]^+$ series.

Table 5: The computed adiabatic and vertical ionization energies of the lowest energy conformers of various glycerol-water clusters.

$(Gly)_x$	$(H_2O)_y$	Vertical/eV	Adiabatic/eV
1	0	10.0	9.2
1	1	9.7	8.7
1	2	9.7	8.7
1	3	9.9	8.8
1	4	9.8	8.5
1	5	10.0	8.7
2	0	9.4	8.4
2	1	9.8	8.5
2	2	9.7	8.8
2	3	9.9	8.6
2	4	9.5	8.3
2	5	10.0	8.4
3	0	9.6	8.6
3	1	9.4	8.2
3	2	9.7	8.7
3	3	9.7	8.4
3	4	9.8	8.3
3	8	9.4	8.1

The adiabatic and vertical ionization energies of the lowest energy conformers are presented in Table 5. Typically, the appearance energies measured experimentally from photoionization efficiency curves for hydrogen bonded systems correspond to vertical ionization. The photoionization efficiency curves for these systems tend to be very smooth without any peaks, making it difficult to correctly ascertain adiabatic ionization energies. Qualitatively, if we compare the measured appearance energies of various fragments shown in Table 1, with the calculated vertical ones (Table 3), they agree reasonably well.

Interestingly, once ionization occurs in these clusters, three barrier-less reactions of the glycerol-water cluster cations are identified from the geometry optimizations, and are illustrated in Figure 6. The first example (Figure 6 (a)) is in a structure of $(Gly)_1 + (H_2O)_1$ obtained from a neutral cluster 2.2 kcal/mol above the lowest energy neutral conformer, which results in a water-mediated proton transfer from the central carbon atom of glycerol to a terminal OH group. The resulting distonic ion has the charge localized on the terminal proton which is strongly hydrogen-bonded (*r*OH = 1.35 Å) to the solvating water molecule, while the relatively stable tertiary radical site is localized at C2. This distonic ion lies 18.6 kcal/mol above the most stable $[Gly(H_2O)]^+$ structure given in Figure 3. Without the solvating water molecule, the distonic Gly^+ ion is not a local minimum at all: it loses water to yield a structure that is 12.7 kcal/mol more stable

than the lowest-lying Gly^+ structure. For a detailed discussion of the post-ionization dynamics of Gly^+, please refer to our earlier work.[23]

The second case shown in Figure 6 (b) is the result of photoionization of a neutral isomer of $(Gly)_1 + (H_2O)_3$ that is 19 kcal/mol above the lowest-energy neutral conformer. After photoionization, barrier-less solvent-assisted fragmentation of the glycerol radical cation occurs, resulting in a nascent hydroxymethyl radical (CH_2OH) separated by 2 Å from the dihydroxyethene cation ($HOCH=CHOH^+$). This direct and nearly complete breaking of a C-C bond to separate the charge and the radical sites was not identified at all in our previous detailed study of glycerol photoionization in the gas phase.[23] The fact that the C-C bond can be broken without a barrier with just three solvating water molecules illustrates the dramatic effect of solvent on the potential energy landscape. Experimental verification is afforded by the trends observed in the $[m/z\ 61(H_2O)_n]^+$ series which mirrors the water composition in the molecular beam.

The third case illustrated in Figure 6 (c) corresponds to the fate of photoionization of the lowest energy conformer of $(Gly)_2 + (H_2O)_5$. Relaxation on this potential energy surface leads to spontaneous proton transfer from photoionized glycerol to one of the water molecules, yielding hydronium and a deprotonated glycerol. This illustrates that acidity of the hydroxyl protons of glycerol can be greatly increased by ionization, to the extent that proton loss to the small cluster of 5 solvating water molecules is barrier-less.

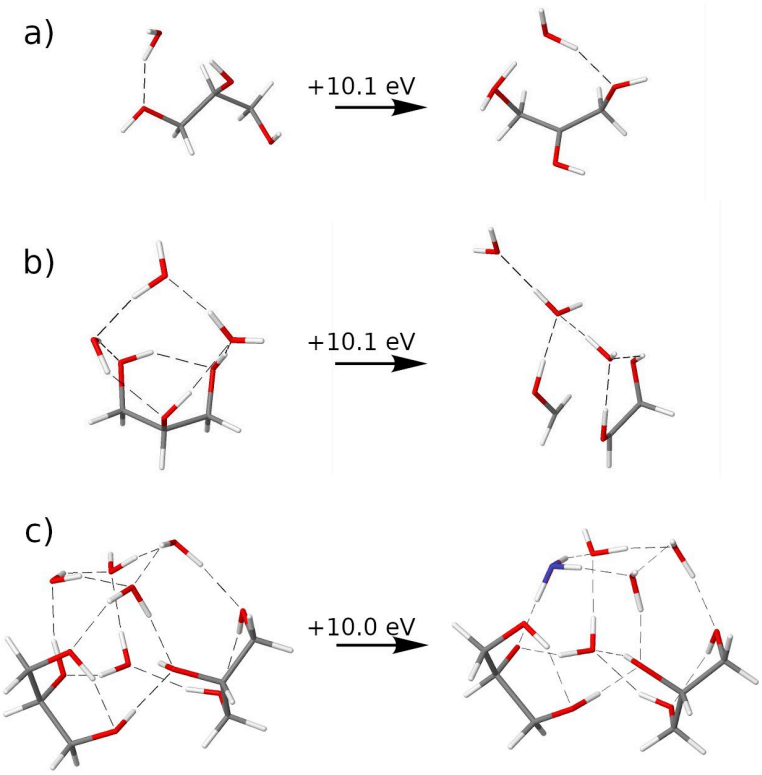

Figure 6: Three theoretical barrier-less (after ionization) reactions of glycerol-water clusters: a) H_2O mediated proton transfer within glycerol, b) hydroxymethyl formation (C-C distance 2.01 Å), and c) hydronium formation (hydronium highlighted in blue).

Conclusion:

Our combined theoretical and experimental study on small glycerol water clusters offers a molecular picture into the hydrogen bond network in these systems. While mass spectrometry samples ions, we can still generate insight into the neutral glycerol water clusters. Previously we have explored the glycerol and water hydrogen bond networks in glycerol-water aerosols using X-ray photoelectron spectroscopy coupled with THz and FTIR spectroscopies.[15] Photoelectron spectroscopy at the X-ray wavelengths employed typically samples the surface of the aerosol (10-20 Å). These are within the dimensions of the clusters studied in this work (see Figure 3). The photoelectron studies revealed that at lower concentrations, glycerol solvates water molecules (see Figure 3 lower left panel $(Gly)_1(H_2O)_5$), while with increasing glycerol concentrations, water tends to be confined by glycerol molecules (see Figure 3 upper right panel $(Gly)_3(H_2O)_1$). From an experimental viewpoint, $[m/z\ 61(H_2O)_n]^+$ trends with solvated water while $[m/z\ 62(H_2O)_n]^+$, $[m/z\ 74(H_2O)_n]^+$ and $[m/z\ 93(H_2O)_n]^+$ series follow confined water with an increase in glycerol concentration. Thus, our supersonic molecular beam generation of small glycerol water clusters followed by photoionization and interpretation of the measured ionization energies and fragmentation

patterns with theoretical insight provides a rich view of hydrogen bonding networks of complex aqueous systems.

From a photoionization dynamics and astrochemistry point of view, our observation of barrier-less fragmentation leading to radicals and distonic ions upon introduction of water, is interesting. It is speculated that UV and VUV processing of alcohol water ices can lead to more complex molecules which might be precursors to biologically relevant molecules.[5, 6] Our work here shows that indeed such speculated pathways can have molecular origins in photoionization. As a general principle, it would appear that barrier-less pathways leading to radicals and ions could be quite ubiquitous in astrochemistry, as we also revealed that acetylene clusters upon photoionization can generate benzene,[33] a precursor to complex carbonaceous structures, while distonic ion structures were observed upon photoionization of naphthalene water clusters.[31] Hence a combination of different molecules in a water matrix in deep space could quite possibly generate biologically relevant chemistry.

Future directions would be to couple vibrational spectroscopy to directly tease out the structures predicted here both in the neutral and ionized states. Already new studies utilizing a VUV free electron laser (FEL) with IR lasers have revealed very interesting structures in pure water clusters.[34-36] These experiments are necessarily limited to the repetition rate of the FEL (between 1-50 Hz). Coupling a CW tunable IR laser to our existing experimental system is a new direction we are in the process of implementing and promises to breathe new life to an ageing synchrotron light source.

Acknowledgements:

This work is supported by the Gas Phase Chemical Physics Program, in the Chemical Sciences Geosciences and Biosciences Division of the Office of Basic Energy Sciences of the U.S. Department of Energy under Contract No. DE-AC02-05CH11231. This research used resources of the Advanced Light Source, which is a DOE Office of Science User Facility under Contract No. DE-AC02-05CH11231. This research used the Lawrencium computational cluster resource provided by the IT Division at the Lawrence Berkeley National Laboratory (Supported by the Director, Office of Science, Office of Basic Energy Sciences, of the U.S. Department of Energy under Contract No. DE-AC02-05CH11231)

Supplementary Information:

The photoionization efficiency curves of series $[m/z\ 61(H_2O)_{0-4}]^+$, $[m/z\ 62(H_2O)_{0-4}]^+$, $[m/z\ 74(H_2O)_{0-3}]^+$, and $[m/z\ 93\ (H_2O)_{0-2}]^+$ series; and the xyz geometry files of the ωB97X-D/6-311+G(2d,p) optimized neutral

glycerol-water clusters. The structures are listed from the lowest to highest energies, with energy in Hartrees listed in the comment line.

References:

1. Weng, L. D.; Stott, S. L.; Toner, M., Exploring Dynamics and Structure of Biomolecules, Cryoprotectants, and Water Using Molecular Dynamics Simulations: Implications for Biostabilization and Biopreservation. *Annu Rev Biomed Eng* **2019,** *21*, 1-31.
2. Hirai, M.; Ajito, S.; Sugiyama, M.; Iwase, H.; Takata, S.; Shimizu, N.; Igarashi, N.; Martel, A.; Porcar, L., Direct Evidence for the Effect of Glycerol on Protein Hydration and Thermal Structural Transition. *Biophys J* **2018,** *115* (2), 313-327.
3. Lessmeier, J.; Dette, H. P.; Godt, A.; Koop, T., Physical state of 2-methylbutane-1,2,3,4-tetraol in pure and internally mixed aerosols. *Atmos Chem Phys* **2018,** *18* (21), 15841-15857.
4. Strongin, R. M., E-Cigarette Chemistry and Analytical Detection. *Annu Rev Anal Chem* **2019,** *12*, 23-39.
5. Abplanalp, M. J.; Gozem, S.; Krylov, A. I.; Shingledecker, C. N.; Herbst, E.; Kaiser, R. I., A study of interstellar aldehydes and enols as tracers of a cosmic ray-driven nonequilibrium synthesis of complex organic molecules. *Proc Natl Acad Sci* **2016,** *113* (28), 7727-32.
6. Turner, A. M.; Kaiser, R. I., Exploiting Photoionization Reflectron Time-of-Flight Mass Spectrometry to Explore Molecular Mass Growth Processes to Complex Organic Molecules in Interstellar and Solar System Ice Analogs. *Acc Chem Res* **2020,** *53* (12), 2791-2805.
7. Towey, J. J.; Soper, A. K.; Dougan, L., Low-Density Water Structure Observed in a Nanosegregated Cryoprotectant Solution at Low Temperatures from 285 to 238 K. *J Phys Chem B* **2016,** *120* (19), 4439-48.
8. Towey, J. J.; Soper, A. K.; Dougan, L., Molecular insight into the hydrogen bonding and micro-segregation of a cryoprotectant molecule. *J Phys Chem B* **2012,** *116* (47), 13898-904.
9. Dashnau, J. L.; Nucci, N. V.; Sharp, K. A.; Vanderkooi, J. M., Hydrogen bonding and the cryoprotective properties of glycerol/water mixtures. *Journal of Physical Chemistry B* **2006,** *110* (27), 13670-13677.
10. Kataoka, Y.; Kitadai, N.; Hisatomi, O.; Nakashima, S., Nature of hydrogen bonding of water molecules in aqueous solutions of glycerol by attenuated total reflection (ATR) infrared spectroscopy. *Appl Spectrosc* **2011,** *65* (4), 436-41.
11. Zelent, B.; Nucci, N. V.; Vanderkooi, J. M., Liquid and ice water and glycerol/water glasses compared by infrared spectroscopy from 295 to 12 K. *J Phys Chem A* **2004,** *108* (50), 11141-11150.
12. Charkhesht, A.; Lou, D.; Sindle, B.; Wen, C.; Cheng, S.; Vinh, N. Q., Insights into Hydration Dynamics and Cooperative Interactions in Glycerol-Water Mixtures by Terahertz Dielectric Spectroscopy. *The Journal of Physical Chemistry B* **2019,** *123*, (41), 8791–8799.
13. Behrends, R.; Fuchs, K.; Kaatze, U.; Hayashi, Y.; Feldman, Y., Dielectric properties of glycerol/water mixtures at temperatures between 10 and 50 °C. *J Chem Phys* **2006,** *124* (14), 144512.
14. Hayashi, Y.; Puzenko, A.; Feldman, Y., Slow and fast dynamics in glycerol–water mixtures. *Journal of Non-Crystalline Solids* **2006,** *352* (42-49), 4696-4703.
15. Weeraratna, C.; Amarasinghe, C.; Lu, W. C.; Ahmed, M., A Direct Probe of the Hydrogen Bond Network in Aqueous Glycerol Aerosols. *J Phys Chem Lett* **2021,** *12* (23), 5503-5511.
16. Callam, C. S.; Singer, S. J.; Lowary, T. L.; Hadad, C. M., Computational analysis of the potential energy surfaces of glycerol in the gas and aqueous phases: Effects of level of theory, basis set, and solvation on strongly intramolecularly hydrogen-bonded systems. *J Am Chem Soc* **2001,** *123* (47), 11743-11754.
17. Kosevich, M. V.; Shelkovsky, V. S., Interactions of glycerol with water in the gaseous state under field ionization conditions. *Rapid Commun Mass Spectrum* **1996,** *10* (4), 435-438.
18. Zavilopulo, A. N.; Shpenik, O. B.; Markush, P. P.; Kontrosh, E. E., Ionization of glycerin molecule by electron impact. *Technical Physics* **2015,** *60* (7), 957-963.
19. Wiens, J. P.; Nathanson, G. M.; Alexander, W. A.; Minton, T. K.; Lakshmi, S.; Schatz, G. C., Collisions of sodium atoms with liquid glycerol: insights into solvation and ionization. *J Am Chem Soc* **2014,** *136* (8), 3065-74.

20. Alexander, W. A.; Wiens, J. P.; Minton, T. K.; Nathanson, G. M., Reactions of Solvated Electrons Initiated by Sodium Atom Ionization at the Vacuum-Liquid Interface. *Science* **2012,** *335* (6072), 1072-1075.
21. Woods, E.; Smith, G. D.; Miller, R. E.; Baer, T., Depth profiling of heterogeneously mixed aerosol particles using single-particle mass spectrometry. *Anal Chem* **2002,** *74* (7), 1642-1649.
22. Frege, C.; Asgari, M.; Steiner, S.; Ferreira, S.; Majeed, S.; Lucci, F.; Frentzel, S.; Hoeng, J.; Kuczaj, A. K., Assessment of Single-Photon Ionization Mass Spectrometry for Online Monitoring of in Vitro Aerosol Exposure Experiments. *Chem Res Toxicol* **2020,** *33* (2), 505-514.
23. Bell, F.; Ruan, Q. N.; Golan, A.; Horn, P. R.; Ahmed, M.; Leone, S. R.; Head-Gordon, M., Dissociative Photoionization of Glycerol and its Dimer Occurs Predominantly via a Ternary Hydrogen-Bridged Ion-Molecule Complex. *J Am Chem Soc* **2013,** *135* (38), 14229-14239.
24. Ahmed, M.; Kostko, O., From atoms to aerosols: probing clusters and nanoparticles with synchrotron based mass spectrometry and X-ray spectroscopy. *Phys Chem Chem Phys* **2020,** *22* (5), 2713-2737.
25. Belau, L.; Wilson, K. R.; Leone, S. R.; Ahmed, M., Vacuum-ultraviolet photoionization studies of the microhydration of DNA bases (Guanine, cytosine, adenine, and Thymine). *J Phys Chem A* **2007,** *111* (31), 7562-7568.
26. Belau, L.; Wilson, K. R.; Leone, S. R.; Ahmed, M., Vacuum ultraviolet (VUV) photoionization of small water clusters. *J Phys Chem A* **2007,** *111* (40), 10075-10083.
27. *Spartan16, Wavefunction Inc.*, Irvine, CA.
28. Halgren, T. A., Merck molecular force field .1. Basis, form, scope, parameterization, and performance of MMFF94. *J Comput Chem* **1996,** *17* (5-6), 490-519.
29. Mardirossian, N.; Head-Gordon, M., Thirty years of density functional theory in computational chemistry: an overview and extensive assessment of 200 density functionals. *Mol Phys* **2017,** *115* (19), 2315-2372.
30. Mackie, C.; Zech, A.; Head-Gordon, M., Effective Two-Body Interactions. *J Phys Chem A* **2021,** *125* (35), 7750-7758.
31. Xu, B.; Stein, T.; Ablikim, U.; Jiang, L.; Hendrix, J.; Head-Gordon, M.; Ahmed, M., Probing solvation and reactivity in ionized polycyclic aromatic hydrocarbon-water clusters with photoionization mass spectrometry and electronic structure calculations. *Faraday Discussions* **2019,** *217*, 414-433.
32. Khistyaev, K.; Golan, A.; Bravaya, K. B.; Orms, N.; Krylov, A. I.; Ahmed, M., Proton Transfer in Nucleobases is Mediated by Water. *J Phys Chem A* **2013,** *117* (31), 6789-6797.
33. Stein, T.; Bandyopadhyay, B.; Troy, T. P.; Fang, Y.; Kostko, O.; Ahmed, M.; Head-Gordon, M., Ab initio dynamics and photoionization mass spectrometry reveal ion-molecule pathways from ionized acetylene clusters to benzene cation. *P Natl Acad Sci USA* **2017,** *114* (21), E4125-E4133.
34. Zhang, B. B.; Yu, Y.; Zhang, Z. J.; Zhang, Y. Y.; Jiang, S. K.; Li, Q. M.; Yang, S.; Hu, H. S.; Zhang, W. Q.; Dai, D. X.; et al, Infrared Spectroscopy of Neutral Water Dimer Based on a Tunable Vacuum Ultraviolet Free Electron Laser. *J Phys Chem Lett* **2020,** *11* (3), 851-855.
35. Zhang, B. B.; Yu, Y.; Zhang, Y. Y.; Jiang, S. K.; Li, Q. M.; Hu, H. S.; Li, G.; Zhao, Z.; Wang, C.; Xie, H.; et al, Infrared spectroscopy of neutral water clusters at finite temperature: Evidence for a noncyclic pentamer. *Proc Natl Acad Sci* **2020,** *117* (27), 15423-15428.
36. Li, G.; Zhang, Y. Y.; Li, Q. M.; Wang, C.; Yu, Y.; Zhang, B. B.; Hu, H. S.; Zhang, W. Q.; Dai, D. X.; Wu, G. R.; et al, Infrared spectroscopic study of hydrogen bonding topologies in the smallest ice cube. *Nat Commun* **2020,** *11* (1). ARTN 5449

TOC Graphic